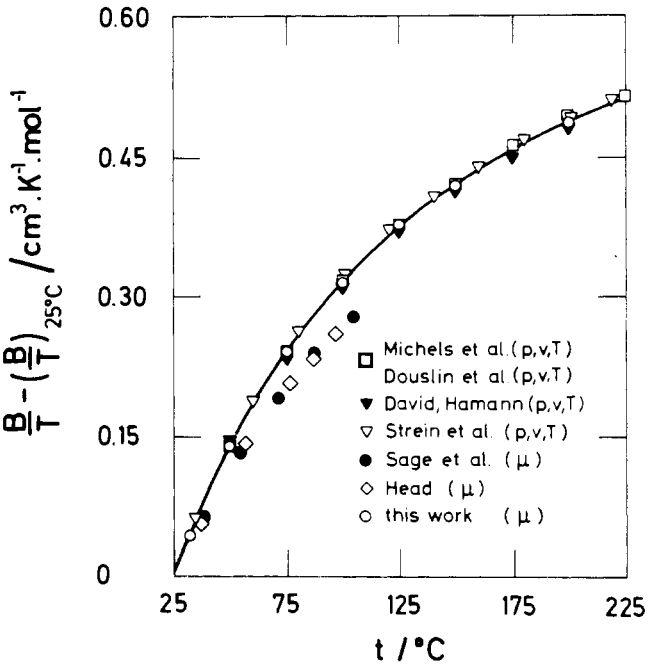

Figure 5. Differences of B/T for ethane from pvT and μ measurements. B = second virial coefficient; T = absolute temperature

$g^{-1} = -0.23083$, $B/J{\cdot}K^{-1}{\cdot}bar^{-1}{\cdot}g^{-1} = +3.0636{\cdot}10^{-4}$ and $C/J{\cdot}K^{2}{\cdot}bar^{-1}{\cdot}g^{1} = -1.5612{\cdot}10^{5}$, this equation represents the ϕ° values of this work within a maximum deviation of 0.42%.

Figure 5 shows that the difference $B/T - (B/T)_{25°C}$ calculated from the μ° values of this work agrees excellently with the results from pvT measurements by Michels et al. (*14*), David and Hamann (*7*), Strein et al. (*18*), and Douslin and Harrison (*8*). For example, the deviations in $\Delta(B/T)$ from Michels and Douslin's results are only 0.7–7.4%. On the other hand, the B/T differences obtained from the μ° values of Sage et al. (*17*) and Head (*10*) deviated by up to 20% from the results of the pvT measurements. This comparison indicates that the Joule-Thomson coefficients determined by these authors are inconsistent with the accepted thermodynamic properties of ethane.

Literature Cited

(1) Barho, W., dissertation, Universität Karlsruhe, Karlsruhe, Germany, 1966, and unpublished calculations.
(2) Bier, K., Ernst, G., Kunze, J., Maurer, G., *Verfahrenstechnik*, **6**, 261 (1972).
(3) Bier, K., Ernst, G., Maurer, G., *J. Chem. Thermodyn.*, **6**, 1027 (1974).
(4) Bier, K., Ernst, G., Kunze, J., Maurer, G., *ibid.*, p 1039.
(5) Chao, J., Wilhoit, R. C., Zwolinski, B. J., *J. Phys. Chem. Ref. Data*, **2**, 427 (1973).
(6) Dailey, B. P., Felsing, W. A., *J. Am. Chem. Soc.*, **65**, 42 (1943).
(7) David, H. G., Hamann, S. D., Proc. Conf. Thermodyn. Transport Properties Fluids, p 74, London, England, 1958.
(8) Douslin, D. R., Harrison, R. H., *J. Chem. Thermodyn.*, **5**, 491 (1973).
(9) Eucken, A., Parts, A., *Z. Phys. Chem.*, **20B**, 184 (1933).
(10) Head, J. F., PhD thesis, Imperial College of Science and Technology, London, England, 1961.
(11) Heuse, W., *Ann. Phys.*, **59**, 86 (1919).
(12) Kilpatrick, J. E., Pitzer, K. S., *J. Res. Nat. Bur. Stand.*, **38**, 191 (1974).
(13) Kistiakowsky, G. B., Rice, W. W., *J. Chem. Phys.*, **7**, 281 (1939).
(14) Michels, A., Van Straaten, W., Dawson, J., **Physica, 20,** 17 (1954).
(15) Pitzer, K. S., *Ind. Eng. Chem.*, **36**, 829 (1944).
(16) Rossini, F. D., Pitzer, K. S., Arnett, R. L., Braun, R. M., Pimentel, G. C., "Selected Values of Physical and Thermodynamic Properties of Hydrocarbons and Related Compounds," p 633, Carnegie Press, Pittsburgh, Pa., 1953.
(17) Sage, B. H., Webster, D. C., Lacey, W. N., *Ind. Eng. Chem.*, **29**, 658 (1937).
(18) Strein, K., Lichtenthaler, R. N., Schramm, B., Schäfer, Kl., *Ber. Bunsenges. Phys. Chem.*, **75**, 1308 (1971).

Received for review October 7, 1974. Accepted August 13, 1975. Financial support by the Deutsche Forschungsgemeinschaft.

Density and Crystallinity Measurements of Liquid and Solid *n*-Undecane, *n*-Tridecane, and *o*-Xylene from 200 to 350K

Jerome G. Hust[1] and Raymond E. Schramm

Cryogenics Division, Institute for Basic Standards, National Bureau of Standards, Boulder, Colo. 80302

Densities of solid and liquid *n*-undecane, *n*-tridecane, and *o*-xylene are reported for temperatures from 200 to 350K. Density increases upon freezing by 13, 13, and 12%, respectively, for these hydrocarbons. The data are presented graphically and are also represented by equations to within the scatter of the data. The uncertainties of the data are 0.2% for the liquid and 1% for the solid state. X-ray examinations revealed that these materials have complex crystalline structures when frozen. Near 200K the main crystal structure is orthorhombic, but several phase transformations occur for each of these materials between 200K and the melting point.

As part of the Skylab program, the Marshall Space Flight Center of the National Aeronautics and Space Administration (MSFC-NASA) required a temperature stabilizing device at several temperatures below ambient. The resulting device, referred to as a thermal capacitor, is simply a container filled with hydrocarbon. Temperature stability is achieved at the freezing point of the hydrocarbon because of the reversible heat reservoir created by its latent heat of fusion. To obtain stability over a range of temperatures, several hydrocarbons, *n*-undecane, *n*-tridecane, and *o*-xylene, have been used. During operation the hydrocarbon container experiences large strains resulting from the volume changes of the hydrocarbon as it cycles between the liquid and solid state. In the past the container has broken after repeated thermal cycles. Therefore, MSFC requested that NBS determine the liquid and solid volume changes of these hydrocarbons at temperatures from 200 to 350K. NBS was also asked to examine the crystallinity of these materials from 200K to their freezing points by X-ray methods.

The following sections present descriptions of the materials, methods of density and specific volume measurements, and X-ray examination. Finally, the results of both density and

[1] To whom correspondence should be addressed.

X-ray measurements are presented in graphical, tabular, and functional form.

Materials

The materials were supplied to NBS by MSFC-NASA and are described as follows: *n*-undecane: $C_{11}H_{24}$, *n*-tridecane: $C_{13}H_{28}$, and *o*-xylene: $C_6H_4(CH_3)_2$; 99.99% pure, 2 ppm residue after evaporation, 15 ppm water, and resistivity = 10^{15} ohm cm at 25°C. No further characterization was performed at this laboratory. Because of the nature of our experimental arrangement, it was impossible to avoid contact of these fluids with atmospheric air. This exposure during measurements undoubtedly influenced the purities and water concentrations, especially that of *o*-xylene. The effect of this change on the final results is believed to be small. Care was taken to avoid any other contamination.

Experimental Methods

Density. Dilatometer and fluid displacement methods were considered to perform the density measurements but are of questionable accuracy for solid measurements. Mercury is often used in these dilatometers but could not be used at low temperatures since it solidifies at −40°C. We decided to use fluid displacement methods for both the solid and liquid states. The liquid densities were determined by weighing a standard glass sphere in air and in the hydrocarbon. This is a standard technique well described by Bowman and Schoonover (*2*). The liquid hydrocarbon was in contact with air, i.e., not outgassed. The density of a glass sphere was measured relative to water from 0° to 60°C. Using these data and a handbook value for the thermal expansion of glass, we obtained

$$\rho = 2.483\ e^{-0.00003\,T}\ \text{g/cm}^3$$

for the density of the glass sphere as a function of temperature, T, in °C. The solid densities were determined by weighing a specimen of hydrocarbon in air and in ethanol. Since densities lower than alcohol were encountered, metal was used in the construction of the specimen holder as ballast. The polyethylene bag, which was used to contain the hydrocarbon, was fastened to a brass disk with wire and epoxy. The disk was fabricated with a fill hole and sealing screw. A copper rod and hook were fastened to the disk for suspension during weighing. Figure 1 illustrates the details of this arrangement.

Densities of the solid hydrocarbon were computed from the experimental data as follows: The observed weight of each part is expressed as the weight in the vacuum minus the buoyant force of air:

$$W_m = m_m g(1 - \rho_a/\rho_m) \quad (1)$$

$$W_{BE} = m_{BE} g(1 - \rho_a/\rho_{BE}) \quad (2)$$

$$W_s = m_s g(1 - \rho_a/\rho_s) = W_{\text{total}} - W_m - W_{BE} \quad (3)$$

The experimentally determined weights and known densities are used to obtain the weight in vacuum, mg. The total weight suspended in ethanol is written as

$$W^{eT}_{\text{total}} = m_m g(1 - \rho_e^T/\rho_m^T) + m_{BE} g(1 - \rho_e^T/\rho_{BE}^T) + m_s g(1 - \rho_e^T/\rho_s^T) \quad (4)$$

The superscript "T" indicates the value at temperature, T.

Equation 4 is solved for ρ_s^T

$$\rho_s^T = \left[m_m \left(1 - \frac{\rho_e^T}{\rho_m^T}\right) + m_{BE}(1 - \rho_e^T/\rho_{BE}^T) + m_s - \frac{W^{eT}_{\text{total}}}{g} \right]^{-1} \rho_e^T m_s \quad (5)$$

where m_s is computed from Equations 1–3 as

$$m_s = \frac{W_{\text{total}} - W_m - W_{BE}}{g(1 - \rho_a/\rho_s)} \quad (6)$$

Since ρ_a/ρ_s is small compared to unity, an approximate value for ρ_s^T is sufficient; otherwise, an iterative solution is necessary.

Density of air was taken to be 0.001 g/cm^3, and the density of ethanol was computed from the equation

$$\rho_e^T = A - 8.461 \times 10^{-4} T + 1.6 \times 10^{-7} T^2 - 8.5 \times 10^{-9} T^3\ \text{g/cm}^3$$

where T is in °C. This equation was presented in ref. *3*. The constant A was evaluated as 0.8062 g/cm^3 by direct density measurements of the ethanol at several temperatures over the temperature range of the solid measurements.

A serious and difficult-to-overcome problem in the solid measurements was the presence of absorbed gases (air) in the specimen. Upon freezing, these dissolved gases formed bubbles, some of which were trapped in the solid and resulted in large density errors. Although no data were found in the literature to confirm this, it appears that the absorption rate of air into these hydrocarbons was very high, thus, further compounding the problem. The amount of dissolved air was reduced as much as possible by vacuum pumping at a pressure above but near the vapor pressure of the fluid for extended periods of time (usually overnight). Alternate freezing and thawing under reduced pressure also were effective in eliminating this gas. The polyethylene bag was measurably permeable to the fluid and air. The error due to permeation of the fluid was reduced to below 0.1% by weighing just prior to freezing. The air permeation was important because of the gas reabsorption into the fluid. A thin latex bag was also tried as a specimen holder. Its permeation rate was larger than that of polyethylene. This permeation problem was minimized by freezing as quickly as possible after degassing. Usually the specimen was sealed from air within a few seconds after degassing and totally frozen within an hour. No gas bubbles were observed in the bag after freezing by this procedure.

The temperature of the fluid bath was controlled for both the liquid and solid density determinations as follows: A copper heat exchanger coil was immersed in the measuring fluid bath. Cold nitrogen boil-off gas from a liquid nitrogen dewar was passed through the copper coil while the temperature of the bath was monitored with conventional glass thermometers. At low temperatures an alcohol-in-glass thermometer accurate to 1°C was used. The boil-off rate of the liquid nitro-

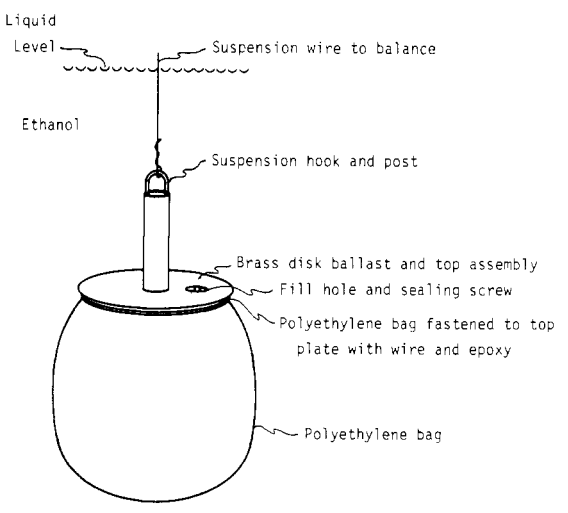

Figure 1. Details of system used to determine solid densities

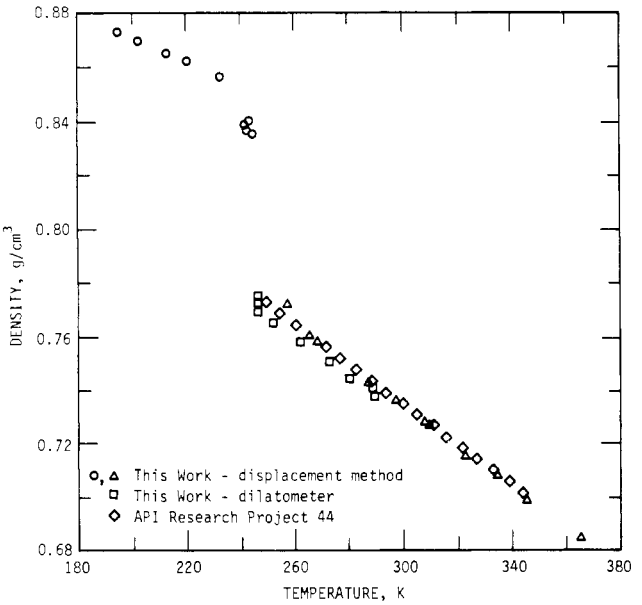

Figure 2. Density of liquid and solid *n*-undecane

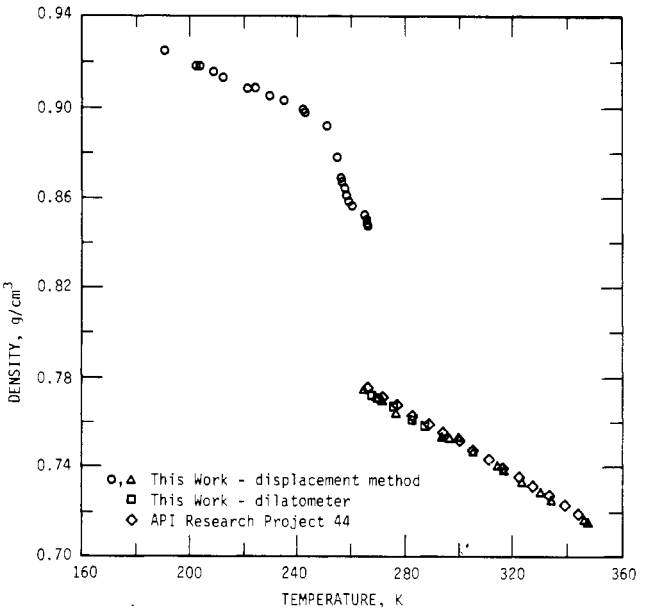

Figure 3. Density of liquid and solid *n*-tridecane

gen dewar was controlled with an electric heater immersed in the liquid nitrogen. Temperatures above ambient were established by placing an electric heater directly in the measuring fluid. The higher temperatures were measured with a mercury-in-glass thermometer accurate to 0.1°C. The measuring fluid was stirred mechanically to assure isothermal conditions, except during the weight determination.

X-ray analysis. The X-ray diffraction specimens of each of the three compounds and a 32 gauge thermocouple were frozen in liquid nitrogen at 76K. These were mounted individually on a commercial X-ray diffractometer and surrounded by an insulated cardboard hood which also enclosed several small reservoirs of liquid nitrogen. By varying the flow rate of gaseous nitrogen into this assembly, it was possible to control specimen temperature.

Results

Density. The densities as computed from Equations 5 and 7 for these materials are illustrated in Figures 2–4 and are listed in Tables I–III. The data were fitted to $\rho = a + bT$ for the pure liquid and solid separately. The coefficients a, b are listed in Table IV. The scatter of the data about this equation was random with a spread of ±0.4% for the liquid data and 0.1% for the solid data. Although it is clear that density is a function of temperature in the solid-liquid transition region, no effort is made to give an analytical description of these data. The objective of this work purposely excluded the very difficult task of determining the density-temperature profile in the transition region. A simplified dilatometer, made from a pipet and calibrated glass cylinder, was used to check the liquid densities as measured by the displacement method and also to check the liquid-to-solid density changes as calculated from the independent solid and liquid measurements. These data are also shown in Figures 2–4. Liquid density data compiled and published by the Thermodynamics Research Center (TRC), Texas A&M University, College Station, Tex. (*1*), are illustrated in Figures 2–4.

The change in density upon freezing is 13, 13, and 12% for *n*-undecane, *n*-tridecane, and *o*-xylene, respectively, as determined by the dilatometer. Since the transition is a function of temperature for *n*-undecane and *n*-tridecane, it is difficult to make a direct comparison of the dilatometer results

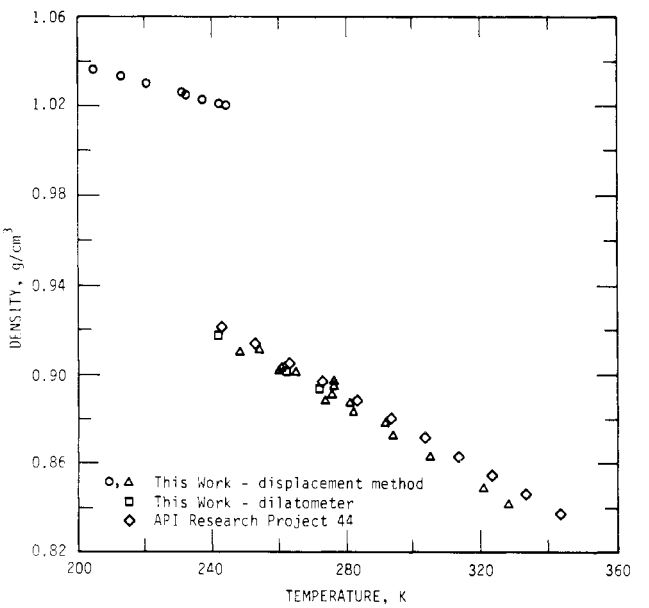

Figure 4. Density of liquid and solid *o*-xylene

Table I. Density Data for *n*-Undecane

Liquid				Solid	
By displacement		By dilatometer			
T, K	Density, g/cm³	*T*, K	Density, g/cm³	*T*, K	Density, g/cm³
365	0.686	290	0.738	195	0.873
345	0.700	281	0.744	203	0.869
335	0.709	273	0.751	214	0.865
323	0.716	263	0.758	221	0.862
310	0.728	252	0.765	234	0.856
308	0.729	247	0.769	233	0.856
298	0.737	289	0.741	244	0.839
288	0.744	247	0.773	243	0.838
269	0.759	247	0.774	245	0.835
266	0.761			243	0.836
258	0.772				

with the changes shown in Figures 2 and 3. In the case of *o*-xylene, there is 1% disagreement between the fluid displacement and dilatometer results.

In the following section on crystallinity, lattice constants are obtained for the orthorhombic phase of *n*-undecane and *n*-tridecane. These constants indicate the unit cell of *n*-undecane is about 17% smaller than *n*-tridecane. Since the molecular weight of *n*-undecane is about 18% smaller, the theoretical densities should be the same to within 1%. This is in agreement with the results shown in Figures 2 and 3 to within the combined uncertainties of the data. This is an estimate, however, since only the orthorhombic phase is considered here.

The estimated uncertainties for these densities are 0.2% for the liquid state and 1% for the solid state. The principal sources of error for the liquid measurements are temperature instability and nonthermal equilibrium. Smaller uncertainties are caused by weighing inaccuracies and discrepancies in the calibration of the glass sphere. The principal source of uncertainty in the solid measurements is the potential presence of undetected gas bubbles trapped in the solid, as discussed previously. The next most important sources of uncertainty are temperature instability and lack of thermal equilibrium.

Table II. Density Data for *n*-Tridecane

Liquid				Solid	
By displacement		By dilatometer			
T, K	Density, g/cm³	*T*, K	Density, g/cm³	*T*, K	Density, g/cm³
293	0.754	287	0.759	244	0.897
282	0.762	283	0.762	230	0.904
270	0.771	282	0.762	222	0.907
265	0.775	282	0.762	213	0.912
277	0.764	282	0.762	203	0.917
277	0.768	276	0.767	192	0.924
296	0.754	270	0.771	204	0.917
305	0.748	272	0.770	209	0.915
314	0.741	268	0.772	225	0.907
323	0.734			236	0.902
334	0.726			243	0.897
348	0.716			252	0.891
346	0.717			255	0.877
330	0.729			257	0.867
316	0.739			258	0.863
300	0.754			260	0.856
				261	0.856
				266	0.850
				267	0.847

Table III. Density Data for *o*-Xylene

Liquid				Solid	
By displacement		By dilatometer			
T, K	Density, g/cm³	*T*, K	Density, g/cm³	*T*, K	Density, g/cm³
292	0.878	272	0.894	205	1.036
281	0.887	262	0.902	214	1.033
276	0.898	242	0.918	221	1.030
276	0.892			233	1.024
265	0.901			238	1.022
255	0.912			243	1.020
261	0.904			245	1.020
248	0.911			232	1.025
260	0.902				
274	0.889				
328	0.842				
320	0.850				
304	0.864				
294	0.874				
282	0.884				
276	0.896				

Table IV. Coefficients, a and b, for $\rho = a + bT$ as Fitted to Liquid and Solid Density Data (Temperature in K)

Material	State	a	b	Temp range, K
n-Undecane	Solid	0.958	−0.000439	193–235
n-Undecane	Liquid	0.955	−0.000734	247–353
n-Tridecane	Solid	1.022	−0.000515	191–253
n-Tridecane	Liquid	0.960	−0.000700	263–353
o-Xylene	Solid	1.124	−0.000426	198–247
o-Xylene	Liquid	1.123	−0.000838	247–348

Crystallinity. The normal paraffins assume several crystalline forms including hexagonal, orthorhombic, monoclinic, and triclinic (*4–7*). Since several of these structures can exist simultaneously, the X-ray patterns can be very complex and are likely to change rapidly with temperature. It is reasonable to expect similar complications with the *o*-xylene.

Three temperature ranges were used to investigate the temperature dependencies of the crystalline forms, and it is apparent that a few degrees can produce a significant change. Several of the X-ray lines for *n*-undecane at about 200K have been indexed as belonging to an orthorhombic lattice with constants of a = 7.3 Å, b = 4.9 Å, and c = 15.5 Å. The dimensions agree reasonably well with the values given by Müller (*4*). This phase is not the only one present, but it does appear to be predominant. At about 220K, the orthorhombic lines are somewhat diminished (with a = 7.7 Å, b = 4.9 Å, c = 15.6 Å), and the crystallite size has decreased as evidenced by a broadening of the lines. A new phase starts to make an appearance at 220K and at 237K seems to be the main structure, whereas the orthorhombic has disappeared. Müller has shown (*5*) that normal paraffins tend to become hexagonal with the approach of the melting point.

The basic X-ray pattern for *n*-tridecane is similar to that for *n*-undecane, and, again, orthorhombic lines are indicated. The lattice constants here are a = 7.6 Å, b = 5.2 Å, c = 16.6 Å at about 200K, and a = 7.8 Å, b = 5.3 Å, c = 16.8 Å at about 247K. These dimensions also agree, within our error, with interpolations from Müller's data (*4*). At 258K, the X-ray pattern shows only a few weak crystalline reflections and is tending toward the broad band structure of an amorphous sample.

The *o*-xylene patterns show a less complicated structure than the paraffins. There are probably still at least two phases present at 209K. A possible tetragonal phase disappears above 221K, but new lines then appear, and, again, there are probably two phases. The story is similar at 230K with the appearance of new lines and the disappearance of old ones.

Summary

Densities of solid and liquid *n*-undecane, *n*-tridecane, and *o*-xylene have been measured from 200 to 350K. The solid data are uncertain to about ±1%. The uncertainty of the liquid data is about ±0.2%.

The X-ray examination indicates that both *n*-undecane and *n*-tridecane, along with *o*-xylene, have complex crystalline structures when frozen. Around 200K the main lattice of the paraffins is orthorhombic, but for all the materials, there are several phase transformations that occur between this temperature and the melting point.

Acknowledgment

We acknowledge the assistance of staff members S. Schmidt, V. Deason, and M. Hiza and NASA project coordinator, J. W. Bransford.

Nomenclature

W_m = weight of metal parts of specimen holder in ambient air = 63.078 g
W_s = weight of specimen in ambient air ≈ 50 g
W_{BE} = weight of bag and epoxy adhesive in ambient air = 1.328 g (a superscript "e" denotes weights in ethanol)
B_m = coefficient of volumetric expansion of metal = $-1/V_m\,\Delta Vm/\Delta T = -54 \times 10^{-6}$, $°C^{-1}$
B_{BE} = coefficient of volumetric expansion of bag and epoxy = -220×10^{-6}, $°C^{-1}$
m = mass, g = acceleration of gravity
ρ_m = density of metal at ambient = m_m/V_m = 8.9 g/cm^3
ρ_{BE} = density of bag and epoxy at ambient conditions = 0.94 g/cm^3
ρ_a = density of air at ambient conditions = 0.001 g/cm^3
ρ_e = density of ethanol

Literature Cited

(1) API Research Project 44 Tables, Thermodynamics Research Center, Texas A&M University, College Station, Tex., 1974.
(2) Bowman, H. A., Schoonover, R. M., *J. Res. Nat. Bur. Stand.*, **71C**, 179 (1967).
(3) Int. Critical Tables, Vol III, p 27, 1928.
(4) Müller, A., *Proc. Roy. Soc. (London)*, **A127**, 417 (1930).
(5) Müller, A., *ibid.*, **A136**, 514 (1932).
(6) Piper, S. H., Malkin, T., *Nature*, **126**, 278 (1930).
(7) Templin, P. R., *Ind. Eng. Chem.*, **48**, 154 (1956).

Received for review October 28, 1974. Accepted August 6, 1975. Contribution of the National Bureau of Standards—not subject to copyright. Work sponsored by NASA, MSFC, Huntsville, Ala.

Thermal Comparator Measurements on Dimethyl Sulfite

Marshall M. Kreitman
University of Dayton, Dayton, Ohio 45469

A thermal comparator was used to obtain a value of 0.178 W m^{-1} °C^{-1} for the thermal conductivity of a high-purity vacuum distilled sample of dimethyl sulfite having a specific density of 1.2083 at 24.8°C.

The thermal conductivity of the organic dimethyl sulfite is of interest because of its potential use as a nonaqueous battery solvent owing to its stability with high-energy density electrodes and its ability to dissolve electrolytes (*2, 8*). Yao et al. (*9*) have measured the melting point (−141°C), the dielectric constant ($\epsilon_{23.3}$ = 22.5), and the viscosity (0.7715 cP at 30°C and 0.4361 cP at 80°C). Kyrides (*4*) has reported a boiling point of 126°C at 760 mm Hg and 52°C at 45 mm Hg, a density of 1.2073 g/cc at 24°C, and an index of refraction of 1.4093 at 20°C for dimethyl sulfite. An exchange current density of 15 mA cm^{-2} for a 1.12 M $LiClO_4$ solution in dimethyl sulfite has been found by Tiedemann and Bennion (*8*).

Mahefkey and Kreitman have noted that the important thermal related properties of battery performance, viz., cell cycle life and cell capacity, as well as electrical efficiency, can be strengthened by operation at lower battery temperatures which they achieved with the introduction of an intercell heat pipe (*5*). The removal of waste heat from a battery is an important design characteristic; therefore, the thermal conductivity of the electrolyte solution is a significant factor in the design and operation of a battery. However, very little information exists on the thermal properties of dimethyl sulfite. To help fill this gap, we have used a thermal comparator to carry out measurements on the room temperature thermal conductivity of the liquid.

The thermal comparator method for obtaining rapid thermal conductivity measurements on solids was introduced by Powell (*6*) in 1957. Subsequent modifications (*7*) have led to the development of a commercial unit (available from the Thermophysical Properties Research Center, Purdue University Research Park, 2595 Yeager Road, W. LaFayette, Ind. 47906), a prototype of which was used in the measurements reported below. The purpose of this paper is to report the thermal conductivity measurement of dimethyl sulfite and to comment on the application of the comparator to the measurement of the thermal conductivity of liquids.

Sample

The liquid sample consisted of approximately 15 cc of commercial grade (Eastman Kodak Co.) dimethyl sulfite at 300K purified by two vacuum distillations. Equal volumes of calibrating liquids were used in the comparator. A westfall balance was used to obtain a value of 1.2083 at 24.8°C for the specific density of the liquid.

Experimental

The thermal comparator method offers a convenient way to obtain the thermal conductivity of an unknown sample to an accuracy of ±5% or better. The instrument registers the rate of cooling experienced by the thermocouple tip of a heated probe when it comes into contact with the surface of a test sample. In general, test samples of different material will draw different amounts of heat from the contact probe according to their thermal conductivity. To avoid undesirable effects which would arise form the probe coming into contact with a liquid sample, the heat conducting ability of the liquid is sensed by the probe through a thin mylar membrane. The membrane is stretched across the bottom of a shallow cylinder, approximately 1.375 in. in diameter, forming a cup $\frac{7}{8}$ in. deep to contain the liquid.

As soon as the temperature sensing tip of the probe comes into thermal contact with the sample, heat is extracted from the tip and creates a temperature difference between tip and probe which is represented by an increasing microvolt reading on the comparator DVM readout control unit. For test samples which have a poor conductivity, the microvolt reading increases to a maximum within several seconds, and afterward it begins to decrease. The approach to the maximum represents an increase in the temperature difference between the probe and the tip. Because the temperature of the probe is carefully controlled, this increase in temperature difference results from a cooling of the tip and a corresponding warming of surface regions of the sample (in